Transactions, SMiRT-22
San Francisco, California, USA - August 18-23, 2013
Division III

SPATIO-FREQUENTIAL CHARACTERIZATION OF NON-UNIFORM TURBULENCE EXCITATIONS USING INVERSE TECHNIQUES : PART 2 - EXTRACTION OF THE PHYSICAL EXCITATION FIELD FROM THE MODAL RESPONSES

Jose Antunes[1], Philippe Piteau[2], Xavier Delaune[2], and Laurent Borsoi[2]

[1] Principal Researcher, Applied Dynamics Laboratory, Campus Tecnológico e Nuclear de Loures, Instituto Superior Técnico, Universidade Técnica de Lisboa, 2686 Sacavem codex, Portugal (jantunes@ctn.ist.utl.pt)
[2] Senior Research Engineer, CEA-Saclay, DEN, DM2S, SEMT, Laboratoire d'Études de Dynamique, F-91191 Gif-sur-Yvette, France (philippe.piteau@cea.fr, xavier.delaune@cea.fr, laurent.borsoi@cea.fr)

ABSTRACT

Following the developments introduced in Part 1 of this work, we pursue in this paper the problem of identifying, from vibratory experiments, the spectral and spatial parameters of turbulent flow excitations with non-uniform velocity profiles. These features are crucial for the predictive dynamical analysis of flow-excited nuclear components, such as steam generators tubes or fuel rods. Our recent work on this topic will be extended here to deal with flows which display significant changes in their spatial properties. Under these conditions, the frequency content of the excitation spectra in different regions of the tube cannot be assumed similar. This departs from the assumption of our previous work and, even if the overall framework of our identification approach was found adequate, the crucial final steps of the identification are formulated here differently. The proposed approach is illustrated with identification results based on realistic numerical simulations of a multi-supported tube subjected to a transverse flow with a triangular velocity profile.

INTRODUCTION

For flow-excited tube bundles, as amply discussed in Part 1, see Antunes et al. (2013b), the need remains for a correct identification of the flow excitation spectral content and spatial distribution, which strongly depends on the velocity profile $V(x)$. Therefore, the topic addressed in this paper is the identification of the spectral and spatial features of random flow excitations. The present research follows the general identification framework recently proposed by Antunes et al. (2013a). The source identification will be performed from a set of measured vibratory responses in the following manner: (1) The modal response spectra and modeshape amplitudes at the measurement locations are first extracted through a blind decomposition of the physical response matrix; (2) The continuous modeshapes are interpolated from the identified values at the measurement locations; (3) The system modal parameters are identified from the modal responses; (4) Inversion from the modal response spectra is performed for identification of the modal excitation spectra; (5) Finally, equivalent physical excitation spectra at different regions of the tube, as well as the flow velocity profile, are estimated.

The first two tasks have been addressed in Part 1, where we have extracted the modal responses $S_{q_n q_n}(f)$ and modeshapes $\phi_n(x)$ from a set of vibratory responses $S_{YY}(x_i, x_j, f)$, $i, j = 1, 2, \cdots, R$, as illustrated in Figure 1. The remaining tasks will be developed in this paper, where we proceed by extracting the modal parameters m_n, f_n and ζ_n from the modal responses. We can then perform an

identification of the modal excitation spectra $S_{F_nF_n}(f)$ from the modal responses $S_{q_nq_n}(f)$. Finally, from the modal excitation spectra, we propose a technique to identify the equivalent excitation spectrum $\bar{\Phi}_{EQ}(f_R)$ as well as the flow velocity profile $u(x)$.

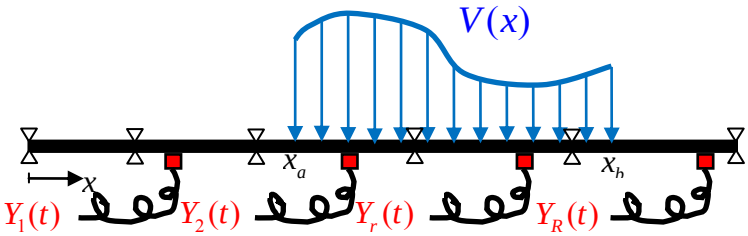

Figure 1. Multi-supported tube subjected to a flow with generic velocity profile $V(x)$.

Several aspects demark the present work from our previous efforts presented in Antunes et al. (2013a), which have been extended here to deal with flows displaying significant changes in their spatial properties $V(x)$. Under these conditions, the frequency content of the excitation spectra in different regions of the tube cannot be assumed similar. This departs from the assumption of our previous work and, even if the overall framework of our identification approach was found adequate, the crucial final steps of the identification are formulated here differently, in a more general manner.

As discussed in Part 1, the proposed approach is illustrated with results based on realistic numerical simulations of a multi-supported tube, for linear supports with no clearances nor friction, subjected to a transverse flow with a triangular velocity profile.

IDENTIFICATION OF THE MODAL EXCITATIONS

Before tackling the problem of identifying the modal excitations $S_{F_nF_n}(f)$ from the modal responses $S_{q_nq_n}(f)$, one must identify the modal parameters m_n, f_n and ζ_n from the modal responses. Actually, only the estimates of the modal masses $\hat{m}_n$ depend on the quality of the estimates of the modeshapes $\hat{\phi}_n(x)$ already obtained. Indeed, the modal masses $\hat{m}_n$ will be estimated by assuming that the mass distribution (including the fluid added mass) $m_0(x)$ is reasonably known a priori. Then:

$$\hat{m}_n = \int_0^L m_0(x)\left[\hat{\phi}_n(x)\right]^2 dx = m_0 \int_0^L \left[\hat{\phi}_n(x)\right]^2 dx \tag{1}$$

where the simpler equation arises because in the present case the mass per unit length is assumed constant. Figure 2 (left-side plot) illustrates the modal masses obtained from the estimated interpolated modeshapes $\hat{\phi}_n(x)$ shown in Figure 6 of Part 1. Comparison with the real values shows that the $\hat{m}_n$ estimates are of very acceptable quality.

Once modal separation is achieved, it becomes easy to identify the other modal parameters by fitting to each modal response curve (either in the frequency-domain or in the time-domain) a SDOF identification algorithm. In the present study we decided to apply a modal identification technique in the time-domain based on the Hilbert Transform $\mathcal{H}[\oplus]$, which is both simple and effective. Extracting the autocorrelation functions for positive time-delays from Figure 8 of Part 1, $G_n(t) \equiv \hat{R}_{q_nq_n}(\tau \geq 0)$, these should follow the free response pattern decay of free SDOF linear oscillators, for modes $n = 1, 2, \cdots, N$ to identify:

$$G_n(t) = G_{n0}\exp\left(-2\pi f_n\zeta_n t\right)\cos\left(2\pi f_n\sqrt{1-\zeta_n^2}\,t\right) \tag{2}$$

We may then compute the corresponding analytic functions:

$$\tilde{G}_n(t) = G_n(t) + i\mathcal{H}\left[G_n(t)\right] = A_n(t)\exp\left(i\theta_n(t)\right) \tag{3}$$

with the amplitude and phase functions:

$$A_n(t) = \left|\tilde{G}_n(t)\right| \quad ; \quad \theta_n(t) = \tan^{-1}\left(\mathcal{H}\left[G_n(t)\right]/G_n(t)\right) \tag{4}$$

and from (2)-(4) it can be shown, see Yang et al. (2003), that:

$$F_1(t) \equiv \frac{d}{dt}\left(\ln\left(A_n(t)\right)\right) = -2\pi f_n(t)\zeta_n(t) \quad ; \quad F_2(t) \equiv \frac{d}{dt}\left(\theta_n(t)\right) = 2\pi f_n(t)\sqrt{1-\zeta_n^2(t)} \tag{5}$$

then, time-averaging (5) within the identification window $t \in [0, T_{ide}]$:

$$\bar{F}_1 \equiv \left\langle F_1(t)\right\rangle = -2\pi\hat{f}_n\hat{\zeta}_n \quad ; \quad \bar{F}_2 \equiv \left\langle F_2(t)\right\rangle = 2\pi\hat{f}_n\sqrt{1-\hat{\zeta}_n^2} \tag{6}$$

so that one obtains the following modal parameter estimates:

$$\hat{\zeta}_n = \left[\frac{(\bar{F}_1)^2}{(\bar{F}_1)^2 + (\bar{F}_2)^2}\right]^{1/2} \quad ; \quad \hat{f}_n = \frac{\bar{F}_2}{2\pi\sqrt{1-\hat{\zeta}_n^2}} \tag{7}$$

One may conclude that the results thus obtained, shown in Figure 2 (center and right-side plots), are again quite satisfying.

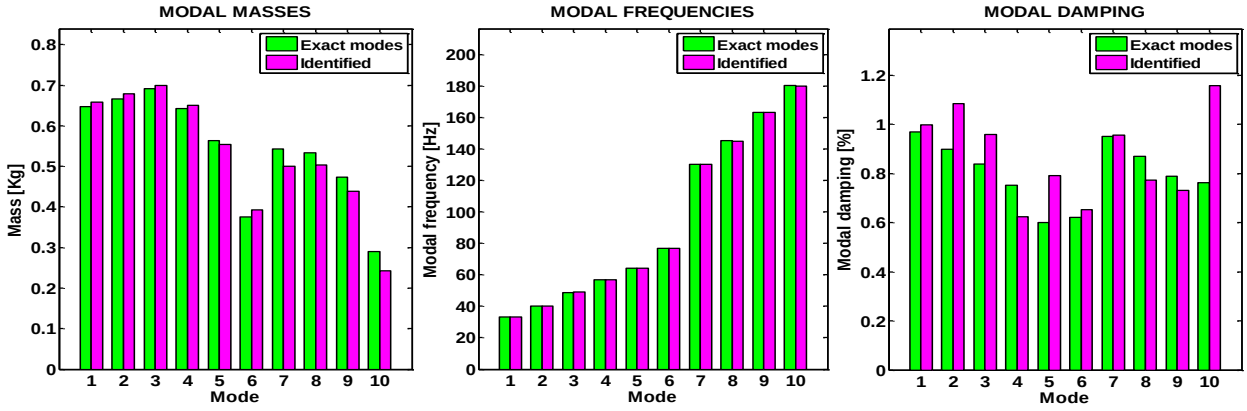

Figure 2. Real and identified modal parameters from the simulated.

We may now estimate the modal forces, which simply stem from formulation:

$$S_{q_nq_m}(f) = H_n(f)H_m^*(f)S_{F_nF_m}(f) \quad ; \quad m,n = 1,2,\cdots,N \tag{8}$$

where $H_n(f) = \left[4\pi^2 m_n\left(f_n^2 - f^2 + 2if f_n\zeta_n\right)\right]^{-1}$. As only auto-spectra are used here, this equation leads to:

$$\hat{S}_{q_nq_n}(f) = \left|\hat{H}_n(f)\right|^2\hat{S}_{F_nF_n}(f) \quad ; \quad n = 1,2,\cdots,N \tag{9}$$

where $\left|\hat{H}_n(f)\right|$ is computed from the estimated modal parameters $\hat{m}_n$, $\hat{f}_n$ and $\hat{\zeta}_n$, while the modal response auto-spectra $\hat{S}_{q_nq_m}(f)$ have also been estimated at the present stage. It is well-known that inversion of (9) may be ill-conditioned, so that some regularization procedure may have to be used. Because in Perotin & Granger (1999) regularization had to be applied, the authors developed an involved implementation of the classic Tikhonov (1977) technique. In the present case, fortunately, we did not find the need for regularization. The results shown in Figure 3, produced through a straight application of (9), are quite satisfying. The only noticeable oddity is the spurious intrusion of mode 12 into some identified

modal excitation spectra, particularly for mode 6, see Figure 7 of Part 1. This artifact is of no consequence, as it can be easily filtered out.

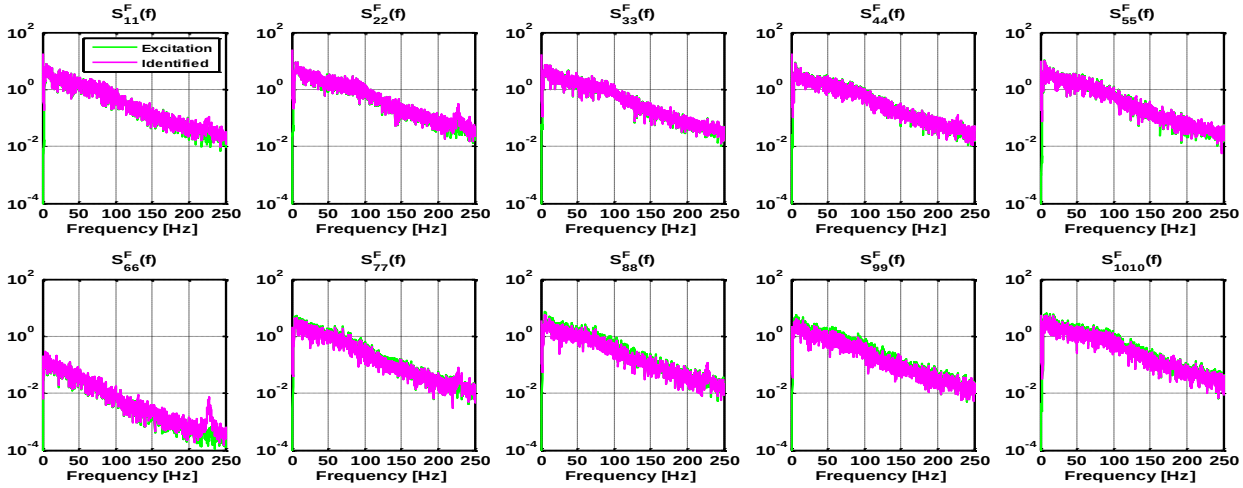

Figure 3. Real and identified auto-spectra of the modal excitations using the modeshapes interpolated from the measurement and support locations.

IDENTIFICATION OF THE PHYSICAL EXCITATIONS

To tackle the final part of the identification problem, in order to find the features of the physical flow excitation from the modal excitation results of Figure 3, these may be worked in various manners. Any identification approach used will obviously depend on what is hypothesized about the unknown excitation field under investigation. Here we will assume that the flow turbulence excitations to be identified actually behave as modeled through the general formulation developed in Part 1. For identification of the unknown excitation field, the space-domain $[0, L]$ will be decomposed in $p = 1, 2, \cdots, P_{ide}$ identification regions, where the "local" average velocities to be identified will be denoted $\hat{V}_p$. For simplicity, we will furthermore consider the velocity profile constant within each section. Then we can approximate the unknown velocity profile by:

$$\hat{V}(x) \approx \sum_{p=1}^{P_{ide}} \hat{V}_p \hat{u}_p(x) \quad \text{with} \quad \hat{V}_p = \frac{1}{L_p} \int_{x_p^i}^{x_p^f} \hat{V}(x) dx \quad \text{and} \quad \hat{u}_p(x) = \begin{cases} 1 & \left(x_p^i \le x \le x_p^f\right) \\ 0 & \left(x \le x_p^i \; ; x \ge x_p^f\right) \end{cases} \tag{10}$$

so that the modal auto-spectra are approximated by:

$$S_{F_n F_n}(f) \approx \sum_{p=1}^{P_{ide}} \left(\frac{1}{2} \rho \hat{V}_p^2 D \right)^2 \frac{D}{\hat{V}_p} \widehat{\Phi}_{EQR}^{T,A} \left(\frac{fD}{\hat{V}_p} \right) \left(\hat{C}_{nn}^p \right)^2 \quad ; \quad n = 1, 2, ..., N \tag{11}$$

with the joint-correlation integrals estimated through:

$$\left(\hat{C}_{nn}^p \right)^2 = 2 \int_{x_p^i}^{x_p^f} \left[\hat{\phi}_n(x) \right]^2 dx \quad ; \quad n = 1, 2, ..., N \quad ; \quad p = 1, 2, \cdots, P_{ide} \tag{12}$$

For compactness, we will write (11) in the form:

$$S_{F_n F_n}(f) \approx \sum_{p=1}^{P_{ide}} \left(\frac{1}{2} \rho \right)^2 D^3 \hat{V}_p^3 \widehat{\Phi}_{EQR}^{T,A} \left(\frac{fD}{\hat{V}_p} \right) \left(\hat{C}_{nn}^p \right)^2 = C \sum_{p=1}^{P_{ide}} \hat{V}_p^3 \widehat{\Phi}_{EQR}^{T,A} \left(\frac{fD}{\hat{V}_p} \right) \left(\hat{C}_{nn}^p \right)^2 \quad ; \quad n = 1, 2, ..., N \tag{13}$$

with parameter $C = \left(\rho / 2 \right)^2 D^3$, assumed known. Equation (13) may be written as well:

$$S_{F_nF_n}(f)=\sum_{p=1}^{P_{ide}}\left(\hat{C}_{nn}^{p}\right)^2\hat{S}_{pp}(f)\quad;\quad n=1,2,...,N \tag{14}$$

where the equivalent physical excitation spectra at the various identification sections are given by:

$$\hat{S}_{pp}(f)=C\hat{V}_p^3\,\hat{\Phi}_{EQR}^{T,A}\left(\frac{fD}{\hat{V}_p}\right)\quad;\quad p=1,2,\cdots,P_{ide} \tag{15}$$

Then, from the knowledge of N modal excitations $S_{F_nF_n}(f)$, $n=1,2,...,N$, one can attempt to identify the various physical excitations $\hat{S}_{pp}(f)$, $p=1,2,\cdots,P_{ide}$, by inverting the set of equations (14):

$$\begin{Bmatrix}\hat{S}_{11}(f)\\ \hat{S}_{22}(f)\\ \vdots\\ \hat{S}_{P_{ide}P_{ide}}(f)\end{Bmatrix}=\begin{bmatrix}\left(\hat{C}_{11}^{1}\right)^2 & \left(\hat{C}_{11}^{2}\right)^2 & \cdots & \left(\hat{C}_{11}^{P_{ide}}\right)^2\\ \left(\hat{C}_{22}^{1}\right)^2 & \left(\hat{C}_{22}^{2}\right)^2 & \cdots & \left(\hat{C}_{22}^{P_{ide}}\right)^2\\ \vdots & \vdots & \ddots & \vdots\\ \left(\hat{C}_{NN}^{1}\right)^2 & \left(\hat{C}_{NN}^{2}\right)^2 & \cdots & \left(\hat{C}_{NN}^{P_{ide}}\right)^2\end{bmatrix}^{+}\begin{Bmatrix}S_{F_1F_1}(f)\\ S_{F_2F_2}(f)\\ \vdots\\ S_{F_NF_N}(f)\end{Bmatrix} \tag{16}$$

where $\left[\otimes\right]^{+}$ stands for the pseudo-inverse of matrix $\left[\otimes\right]$. In compact notation, (16) reads:

$$\left\{\hat{S}_{pp}(f)\right\}=\left[\left(\hat{C}_{nn}^{p}\right)^2\right]^{+}\left\{S_{F_nF_n}(f)\right\} \tag{17}$$

Notice that (17) may in principle be applied for every frequency in the range of interest. However, because of the random nature of turbulence spectra, the straight inversion thus performed will lead to poor results. We have found that, before inverting, it is advantageous to further smooth the modal excitation spectra through averaging within a moving frequency window. In the limit, integration of the spectral functions in (14) within the full frequency range of interest leads to the interesting result:

$$\int_0^{f_{\max}}S_{F_nF_n}(f)df=\sum_{p=1}^{P_{ide}}\left(\hat{C}_{nn}^{p}\right)^2\int_0^{f_{\max}}\hat{S}_{pp}(f)df\quad;\quad n=1,2,...,N \tag{18}$$

or:

$$\sigma_{nn}^2=\sum_{p=1}^{P_{ide}}\left(\hat{C}_{nn}^{p}\right)^2\hat{\sigma}_{pp}^2\quad;\quad n=1,2,...,N \tag{19}$$

hence, from (16), the global formulation:

$$\begin{Bmatrix}\hat{\sigma}_{11}^2\\ \hat{\sigma}_{22}^2\\ \vdots\\ \hat{\sigma}_{P_{ide}P_{ide}}^2\end{Bmatrix}=\begin{bmatrix}\left(\hat{C}_{11}^{1}\right)^2 & \left(\hat{C}_{11}^{2}\right)^2 & \cdots & \left(\hat{C}_{11}^{P_{ide}}\right)^2\\ \left(\hat{C}_{22}^{1}\right)^2 & \left(\hat{C}_{22}^{2}\right)^2 & \cdots & \left(\hat{C}_{22}^{P_{ide}}\right)^2\\ \vdots & \vdots & \ddots & \vdots\\ \left(\hat{C}_{NN}^{1}\right)^2 & \left(\hat{C}_{NN}^{2}\right)^2 & \cdots & \left(\hat{C}_{NN}^{P_{ide}}\right)^2\end{bmatrix}^{+}\begin{Bmatrix}\sigma_{11}^2\\ \sigma_{22}^2\\ \vdots\\ \sigma_{NN}^2\end{Bmatrix} \tag{20}$$

or, in compact notation:

$$\left\{\hat{\sigma}_{pp}^2\right\}=\left[\left(\hat{C}_{nn}^{p}\right)^2\right]^{+}\left\{\sigma_{nn}^2\right\} \tag{21}$$

Notice that the inversion matrix in (16) and (20) is the same and, while the condition $P_{ide} \leq N$ is needed for the well-posedness of these inverse problems, it is not obvious which actual values should be actually adopted. It seems plausible to use $P_{ide} = N$, in order to get the best possible spatial resolution for a given number N of identified modal responses. Under such conditions, one may easily compute some measure of the numerical condition of matrix $\left[\left(\hat{C}_{nn}^{p}\right)^{2}\right]$ as a function of the number of modes N used in building it. Figure 4 shows the results thus obtained, from the real modeshapes and the identified modeshapes obtained in Part 1, with the condition number here defined as the ratio between the smallest and the largest singular values of the inversion matrix, $C_N = \sigma_{\min}/\sigma_{\max}$, these being obtained from a Singular Value Decomposition (SVD) of $\left[\left(\hat{C}_{nn}^{p}\right)^{2}\right]$ for increasing number of terms. Notice that, with this definition of C_N, a perfectly conditioned matrix leads to $C_N = 1$, while a singular matrix implies $C_N = 0$. The typical decreasing of C_N as N increases is displayed by Figure 4, however using a very small number of modes would obviously lead to very crude results. For higher values of $P_{ide} = N$, one can notice fluctuations in C_N and, for the modeshapes of the present system, there is a value ($N = 6$) more favorable than others (for instance $N = 7$).

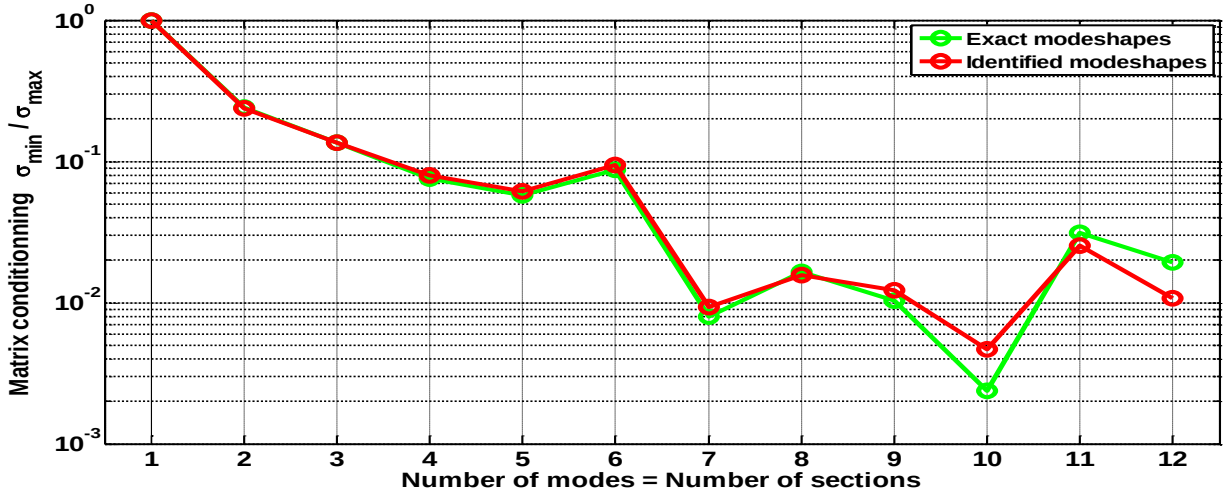

Figure 4. Condition number of the inversion matrix as a function of the number of modes used.

Another important point is that, by definition, all the excitation spectra $\hat{S}_{pp}(f)$ to identify, as well as the corresponding variances $\hat{\sigma}_{pp}^{2}$, must be strictly positive. Then, we may expect to obtain better estimations by replacing the linear formulation (16)-(17) by a nonlinear one such that positive constraining on the solution is enforced. The following optimization procedure is then formulated: Find vector $\{S_{pp}(f)\}$ that minimizes the following quadratic error norm subject to the inequality constraints:

$$\varepsilon_S(f) = \left\| \left[\left(\hat{C}_{nn}^{p}\right)^{2}\right]\{S_{pp}(f)\} - \{S_{F_nF_n}(f)\} \right\|^{2} \quad ; \quad S_{pp}(f) \geq 0 \quad \forall p, f \tag{22}$$

which constitutes a so-called non-negative least-squares problem, see Lawson & Hanson (1974). It has been shown that, although nonlinear, problem (22) always converges to a solution. Concerning the identification of the spectral variances $\hat{\sigma}_{pp}^{2}$, a similar procedure may be adopted instead of using the straight inversion (20)-(21):

$$\varepsilon_\sigma = \left\| \left[\left(\hat{C}_{nn}^{p} \right)^2 \right] \left\{ \hat{\sigma}_{pp} \right\} - \left\{ \sigma_{nn} \right\} \right\|^2 \quad ; \quad \hat{\sigma}_{pp} \geq 0 \quad \forall p \tag{23}$$

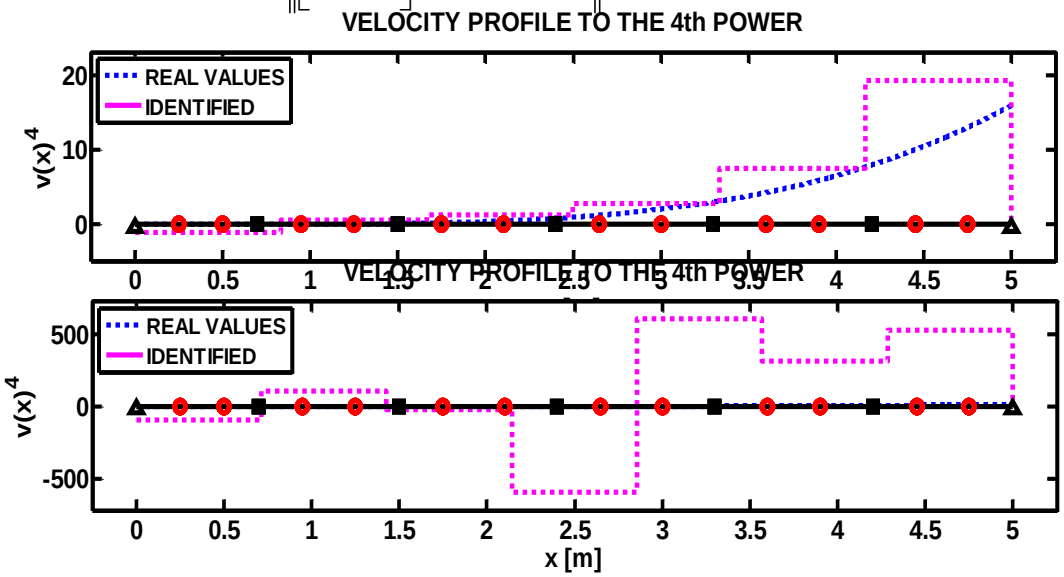

Figure 5. Estimation of $\hat{v}_p^4$ from the straight pseudo-inversion (21):

$P_{ide} = N = 6$; $P_{ide} = N = 7$.

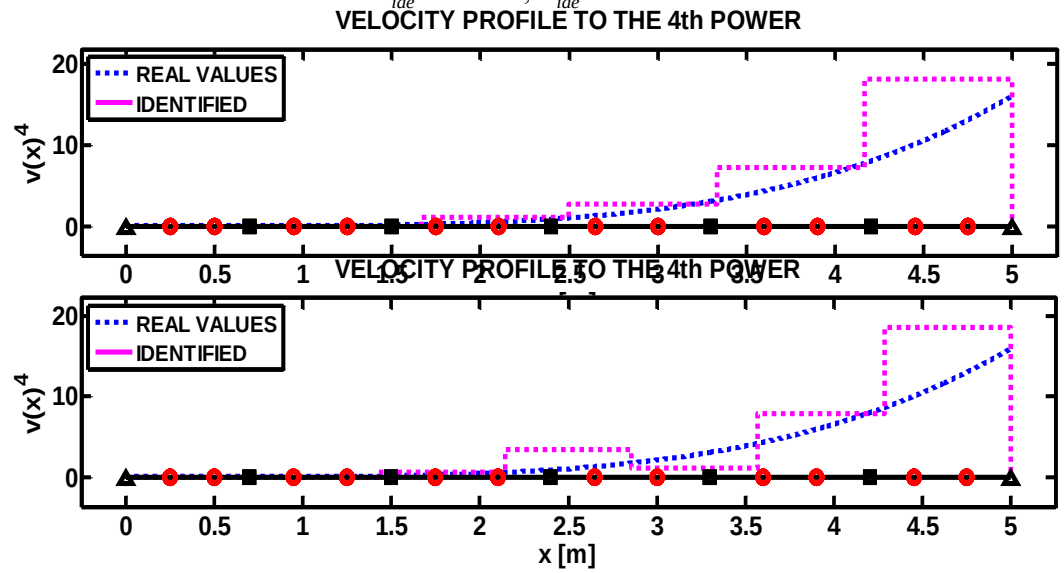

Figure 6. Estimation of $\hat{v}_p^4$ from the non-negative least-squares inversion (23):

$P_{ide} = N = 6$; $P_{ide} = N = 7$.

As an additional remark note that, from (15), one obtains:

$$\hat{\sigma}_{pp}^2 = C\hat{V}_p^3 \int_0^{f_{\max}} \hat{\Phi}_{EQR}^{T,A}\left(\frac{fD}{\hat{V}_p} \right) df = C\hat{V}_p^3 \frac{\hat{V}_p}{D} \sigma_\Phi^2 = \left(\frac{1}{2} \rho D \right)^2 \hat{\sigma}_\Phi^2 \hat{V}_p^4 \quad ; \quad p = 1, 2, \cdots, P_{ide} \tag{24}$$

with the variance of the dimensionless excitation spectrum:

$$\hat{\sigma}_\Phi^2 = \int_0^{f_{R\max}} \hat{\Phi}_{EQR}^{T,A}\left(f_R \right) df_R \tag{25}$$

so that, if we assume that the same dimensionless excitation spectrum applies everywhere along the tube, one obtains the useful result:

$$\hat{V}_p^4 = \frac{\hat{\sigma}_{pp}^2}{\left(\frac{1}{2}\rho D\right)^2 \hat{\sigma}_\Phi^2} \quad \Rightarrow \quad \hat{V}_p \propto \sqrt[4]{\hat{\sigma}_{pp}^2} \quad ; \quad p = 1, 2, \cdots, P_{ide} \tag{26}$$

which provides a convenient relation for estimating the flow velocity profile, after a suitable normalization of the results (26). We thus define the global velocity profile $\hat{v}_p$ such that $(1/L)\sum_{p=1}^{P_{ide}} \hat{v}_p L_p = 1$.

Figures 5 and 6 illustrate the estimates of $\hat{v}_p^4$ from (26) for two consecutive values of $P_{ide} = N = 6$ and 7, first using the straight inversion formulation (21), then using the non-negative least-squares formulation (23). The results shown in Figure 5, obtained through the straight pseudo-inversion (21), highlight the influence of the system conditioning already pointed by Figure 4. It is clear from these plots that $P_{ide} = N = 6$ leads to a much better estimation of $\hat{v}_p^4$, while $P_{ide} = N = 7$ produces meaningless results. On the other hand, the results shown in Figure 6 demonstrate that the non-negative least-squares procedure (23) is more robust, always leading to better and more physical results. Figure 7 illustrates the estimated velocity profile $\hat{v}_p$ obtained from the result of Figure 6, with $P_{ide} = N = 6$ which is adequate.

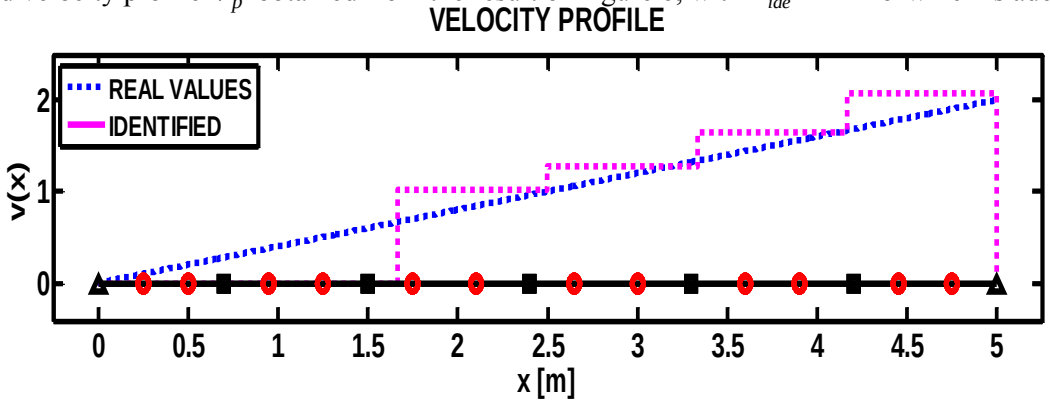

Figure 7. Estimation of the velocity profile $\hat{v}_p$ from the non-negative least-squares inversion (23).

Using formulation (22) we obtained the physical spectra at the $P_{ide} = 6$ sections of the tube, as illustrated in Figure 8. Shown are the original physical excitation spectra at the $P_{cal} = 12$ computational tube sections (blue), as well as the identified physical excitation spectra at the identification tube sections $p = 4, 5$ and 6 (magenta), where flow velocity is higher. The identified excitation spectra are not shown for the first three identification sections because, in agreement with the results of Figure 7, the identified excitations $\hat{S}_{pp}(f)$ in regions $p = 1$ and 2 are nearly nil, while in region 3 it is always lower than $\hat{S}_{44}(f)$ but changes erratically with frequency. This means that, under difficult conditions such as the example in this paper, one cannot estimate the excitation spectra at regions of the tube where the flow velocity is significantly lower. In retrospect, such result is far from surprising. Also important in Figure 8 is the fact that the identified excitation spectra $\hat{S}_{44}(f) \sim \hat{S}_{66}(f)$ well reflect the different spectral content of the local excitation, which stems from the local change in the reduced frequency connected with the flow velocity profile.

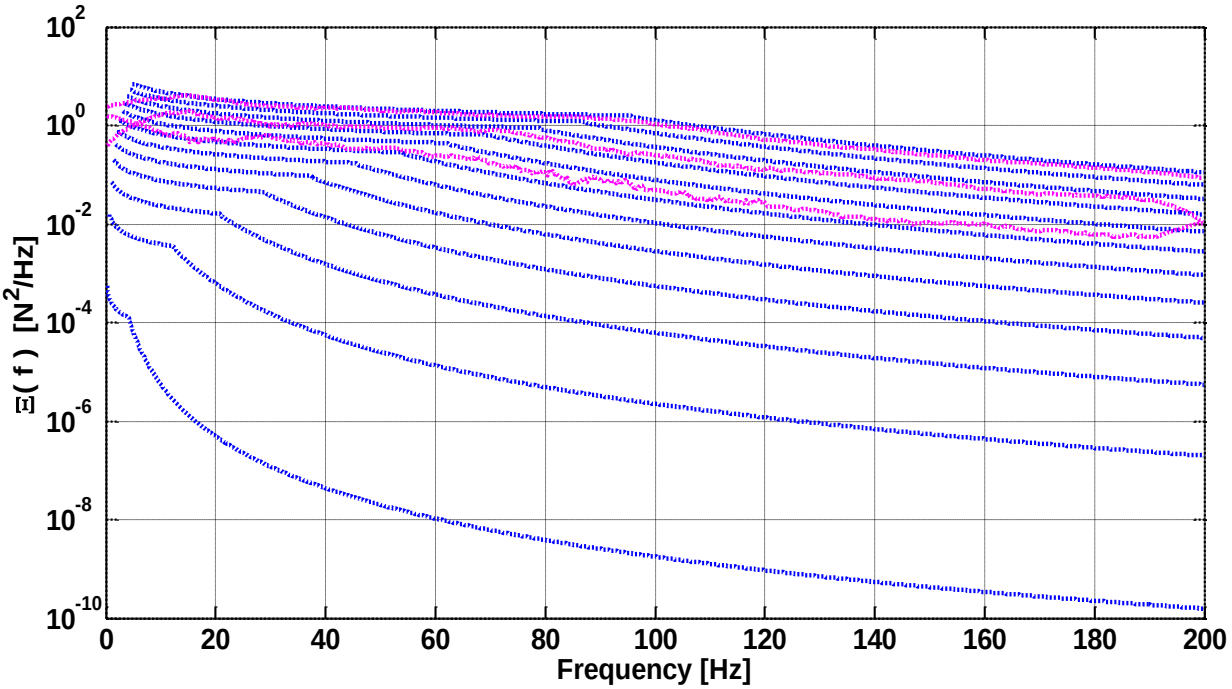

Figure 8. Equivalent physical excitation spectra at the various tube sections for $P_{ide} = N = 6$: Original physical excitation spectra at the $P_{cal} = 12$ computational tube sections (blue); Identified physical excitation spectra at tube sections $p = 4, 5$ and 6 (magenta).

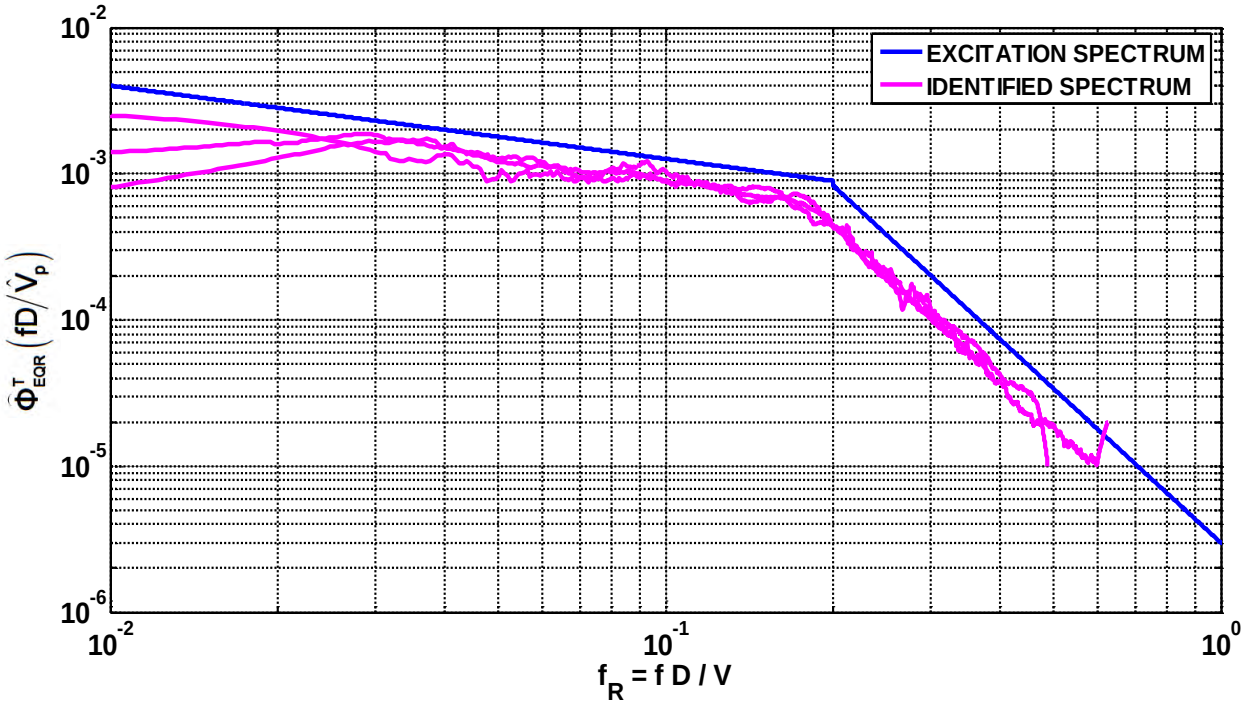

Figure 9. Real and identified equivalent reduced excitation spectra $\hat{\Phi}^{T}_{EQR}\left(fD/\hat{V}_p \right)$ extracted from the physical estimates $\hat{S}_{44}(f) \sim \hat{S}_{66}(f)$.

At this stage one can now estimate the dimensionless spectrum $\hat{\Phi}^{T}_{EQR}\left(fD/\hat{V}_p \right)$ by reducing the equivalent physical excitations $\hat{S}_{pp}(f)$ using formulation (15), provided that the physical flow velocities are $\hat{V}_p$ known at the various tube sections. Unfortunately, these cannot be inferred directly from the identification results, which only provide the dimensionless velocity profile $\hat{v}_p$. Actually, to obtain the physical velocities, some additional information must be supplied, such as a measured flow rate, or some local flow velocity measurement, which enable a scaling of the $\hat{V}_p$.

In Figure 9 we plot the results thus obtained from $\hat{S}_{44}(f) \sim \hat{S}_{66}(f)$, by estimating the physical velocity field $\hat{V}_p$ from the identified profile $\hat{v}_p$ in order to obtain the global flow rate of the original system. The identified results plotted display a small frequency and amplitude bias, when compared with the real equivalent dimensionless spectrum used for performing the simulations. This is due to the differences between the estimated flow velocity profile and the real velocity field, shown in Figure 7. Nevertheless, accounting for difficulties of the identification problem, the results obtained are quite satisfying.

CONCLUSION

Following from the results presented Part 1, we have developed in this paper an extensive approach for extracting the relevant structural and excitation dynamical features of a flow-excited structure. The proposed technique enables the identification of the turbulence excitation field, from a set of vibratory measurements, using a minimum of a priori information on both the structure and the flow. The identified items include the structure modal parameters, as well as the spectral and spatial characteristics of the distributed flow excitation. The results obtained so far, based on realistic numerical simulations of a multi-supported tube subjected to a non-uniform flow velocity field, are quite promising. From the results presented here, identification of the structural modal parameters, of the modal responses and excitations, as well as of the turbulence excitation spectrum, appears feasible, accurate and robust enough.

REFERENCES

Antunes, J., Borsoi, L., Delaune, X., Piteau, P. (2013a). "Identification of the Turbulence Force Field Excitation From a Set of Vibratory Responses of a Multi-Supported Tube", Paper 98146, *Proceedings of the ASME 2013 Pressure Vessel and Piping Conference (PVP2013)*, July 14-18, 2013, Paris, France.

Antunes, J., Piteau, P., Delaune, X., Borsoi, L. (2013b), "Spatio-Frequential Characterization of Turbulence Excitations Using Inverse Techniques : Part 1 - Extraction of the Modal Responses From the Vibratory Measurements", *22th International Conference on Structural Mechanics in Reactor Technology (SMiRT-22)*, 18-23 August, 2013, S. Francisco, USA.

Lawson, C.L., Hanson, R.J. (1974). "*Solving Least Squares Problems*", Prentice-Hall, Englewood Cliffs, USA.

Perotin, L., Granger, S. (1999). "An Inverse Method for the Identification of a Distributed Random Excitation Acting on a Vibrating Structure. Part 2: Flow-Induced Vibration Application", Mechanical Systems and Signal processing , Vol. 13, pp. 67-81.

Tikhonov, A.N., Arsenin, V.Y. (1977). "*Solutions of Ill-Posed Problems*", Wiley, New York, USA.

Yang, J.N, Lei, Y., Pan, S.W., Huang, N. (2003). "System Identification of Linear Structures Based on Hilbert-Huang Spectral Analysis. Part 1: Normal Modes", *Earthquake Engineering and Structural Dynamics*, Vol. 32, pp.1443-1467.